Switchable Josephson junction based on interfacial exchange field

Juan Pedro Cascales, Yota Takamura (iD), Gregory M. Stephen (iD), Don Heiman, F. Sebastian Bergeret, and Jagadeesh S. Moodera

View Online   Export Citation   CrossMark

ARTICLES YOU MAY BE INTERESTED IN

Switchable Josephson junction based on interfacial exchange field

View Online   Export Citation   CrossMark

Juan Pedro Cascales,[1,2,a)] Yota Takamura,[1,2,3,b)] (iD) Gregory M. Stephen,[4] (iD) Don Heiman,[4] F. Sebastian Bergeret,[5,6,c)] and Jagadeesh S. Moodera[1,2,7,d)]

AFFILIATIONS

[1] Francis Bitter Magnet Laboratory, Massachusetts Institute of Technology, Cambridge, Massachusetts 02139, USA

[2] Plasma Science and Fusion Center, Massachusetts Institute of Technology, Cambridge, Massachusetts 02139, USA

[3] School of Engineering, Tokyo Institute of Technology, Tokyo 152-8552, Japan

[4] Department of Physics, Northeastern University, Boston, Massachusetts 02115, USA

[5] Centro de Fisica de Materiales (CFM-MPC), Centro Mixto CSIC-UPV/EHU, Manuel de Lardizabal 4, E-20018 San Sebastian, Spain

[6] Donostia International Physics Center (DIPC), Manuel de Lardizabal 5, E-20018 San Sebastian, Spain

[7] Physics Department, Massachusetts Institute of Technology, Cambridge, Massachusetts 02139, USA

a) Electronic mail: jcasc_87@mit.edu
b) Electronic mail: takamura@ee.e.titech.ac.jp
c) Electronic mail: sebastian_bergeret@ehu.eus
d) Electronic mail: moodera@mit.edu

ABSTRACT

We demonstrate exchange field switchable Josephson junctions where the Josephson tunneling between two superconducting layers (Nb and NbN) could be controlled by the relative magnetic alignment of two GdN ferromagnetic insulator layers sandwiching the Nb layer. The junction's working principle is based on the control of the superconducting state of one of the layers by means of the interfacial exchange field of the magnetic GdN layers. At zero field and low temperatures, the ground state of the junctions corresponds to an antiferromagnetic configuration of the two GdN layers that coexist with the superconducting state of the Nb layer. By applying an external field, the GdN layers are switched to a parallel configuration, thereby suppressing the superconductivity in Nb and hence the Josephson current via interfacial exchange. This switchable Josephson junction may be useful for integrated superconducting spintronics and quantum circuits.

Published under license by AIP Publishing. https://doi.org/10.1063/1.5050382

The Josephson junction (JJ) is a versatile device which has found widespread application as field sensors, as measurement standards, or in quantum computing, among others.[1–3] It consists of superconducting electrodes separated by a non-superconducting link (insulator, normal metal, etc) in which a (Josephson) current flows without dissipation.

There is particular interest in the study of Josephson junctions with magnetic interlayers. The interplay between the superconducting correlations and the exchange field in ferromagnetic materials leads to striking phenomena such as $0-\pi$ transition,[4] long range triplet superconductivity,[5] and anomalous Josephson currents.[6] These phenomena and the ability of JJs to switch between super- and normal currents with high reproducibility and at high rates make magnetic Josephson junctions attractive for the emerging field of superconducting spintronics,[7] building of cryogenic memories,[8] and qubits for quantum computers.[9]

In this context, the combination of ferromagnetic insulators (FIs) and superconductors can be very useful. On the one hand, the strong interfacial exchange field (IEF) due to s-d and s-f exchange between the conducting electrons of the SC and the localized magnetic moments of the FIs leads to a full development of the triplet component[5] and spin-dependent density of states.[10–13] On the other hand, because there is no leakage of Cooper pairs into the FI, the superconducting gap is quite robust, and its magnitude is mainly controlled by the strength of the IEF via the paramagnetic effect. FI bilayers offer exceptionally high magnetic fields localized at atomically sharp

interfaces.[14] For a FI such as GdN, which involves the rare-earth element Gd, the localized f electrons provide the IEF which in a superconductor can propagate over the superconducting coherence length.[12] This exchange field is equivalent to a space inhomogeneous Zeeman field. By sandwiching a SC film between two such magnetic layers and keeping the SC layer's thickness below the coherence length, the effect of the exchange interactions at each interface sums up and can be greatly enhanced. The use of FIs has been recently shown to result in the passive control of superconducting or topological insulator layers in bilayers or spin valves.[13–16] Moreover, an FI located between two superconducting electrodes may serve as a spin-filter, giving rise to spin-filtering Josephson junctions.[12,17] Spin filtering Josephson junctions may exhibit a new type of 0–π transition, even pure triplet currents,[18] and anomalous Josephson currents (φ_0-junctions).[19]

In this letter, we report on the investigation of FI/SC/FI/SC Josephson junctions with a built-in exchange driven magnetic switch. The proposed *switchable Josephson junction* device is based on the IEF induced in a superconductor sandwiched between two FI layers. In the FI/SC/FI structure, defined as a superconducting spin valve (SSV), the superconducting transition temperature T_C of the SC spacer depends on the relative orientation of the magnetization of the two FI layers,[20] referred to as the superconducting spin switch effect (SSE).[14] We find that at zero field, the ground state corresponds to an AP configuration of the magnetization M in the FI layers. In this configuration, the net IEF in the superconductor between the FI layers cancels out and does not affect the superconductivity, allowing a Josephson current to flow. By applying a relatively small magnetic field, we can switch the two FI layers towards a parallel (P) alignment of magnetization. In this case, the average IEF experienced by the Cooper pairs destroys superconductivity in the SC spacer layer and consequently no supercurrent flows. Thus, the combination of the SSE effect and a FI tunneling barrier results in a passively controlled Josephson junction behavior that could be used as a non-volatile memory and logic for superconducting spintronics based on IEF. Moreover, our device could take us towards the full-triplet Josephson junction which would include a third FI layer.[18]

The samples were fabricated by reactive sputtering in an ultra-high vacuum (UHV) system on thermally oxidized Si substrates at room temperature starting with a 1 nm thick seed layer of Al_2O_3. As shown in Fig. 1(a), the layer sequence of the sample is AlN(5)/NbN(10)/GdN(3)/Nb(10)/GdN(3)/AlN(1)/Al(20) with the numbers in parentheses corresponding to the thickness in nm. In these structures, the SC electrodes (NbN and Nb) are separated by a 3 nm GdN tunnel barrier. The second GdN layer situated over the Nb layer, together with the tunneling barrier, sandwiches the Nb layer allowing us to control its superconducting state via the relative magnetic configuration (P or AP) of the GdN magnetic moments. The optimum thicknesses of both GdN layers were arrived at by systematically fabricating junctions with different Nb and GdN thicknesses, as well as by different growth conditions, until Josephson tunneling was observed. The combination of a thin AlN layer followed by a thick Al layer was found to be the best capping to protect samples from degradation while preserving vertical transport.
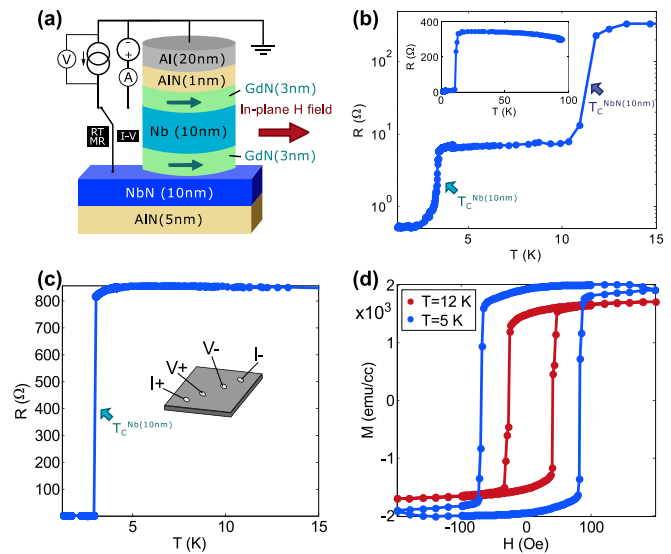

FIG. 1. (a) Schematic of the sample structure and transport measurements. The junctions are circular pillars of diameters ranging from 10 to 80 μm. (b) Resistance vs temperature at zero field (ZFC) of a 10 μm device at a current bias of 10 μA. Two drops are observed at $T = 11.3$ K and $T = 3.2$ K, corresponding to the superconducting critical temperature of the 10 nm NbN ($T_C^{NbN(10)}$) and 10 nm Nb ($T_C^{Nb(10)}$) films, respectively. The inset depicts R vs T up to higher temperature. (c) R vs T (ZFC) of an unpatterned layered structure in which only the Nb film has been contacted, with $T_C = 3$ K. (d) M-H loops for the unpatterned sample at 5 and 12 K, showing only one coercive field for the GdN sandwich.

After deposition, the samples were patterned by optical lithography and ion milling into circular junctions with diameters ranging from 10 to 80 μm. The milling was carried out down to the bottom NbN layer, leaving it intact. The pillar structure was protected by 20 nm of Al_2O_3 filler, and a 100 nm thick Al contact pad of 1 mm^2 area was fabricated through an additional lithography/sputtering step. Independent electrical contact with indium was made to each SC layer via the top electrode pad (Nb) and by scratching a corner of the wafer to expose NbN.

Figure 1(b) plots resistance vs temperature, zero-field cooled (ZFC), of a 10 μm device (essentially a 3-terminal measurement), with an applied current I = 10 μA. Two clear drops in resistance occur at the superconducting transition temperatures of the 10 nm NbN layer ($T_C^{NbN(10)} = 11.3$ K) and the 10 nm Nb layer ($T_C^{Nb(10)} = 3.2$ K), where each T_C was taken as the mid-point of each resistive transition. The reduced value of T_C of the Nb layer (up to 7.5 K for pure 10 nm Nb[21]) is mainly credited to the proximity of the magnetic layers. The highest resistance value achieved before the first SC transition is 343 Ω. The drop from 343 to 7 Ω when NbN becomes SC can be accounted for in order of magnitude by the spread resistance in the NbN layer experienced between the scratched indium contact and the bottom pillar. When the SC transition of the Nb layer takes place, the resistance further drops down to ~0.5 Ω, which we attribute to the occurrence of Josephson tunneling. The residual 0.5 Ω resistance could be ascribed to a rougher top AlN/GdN layer. Figure 1(c) shows R vs T (ZFC) of the 10 nm Nb film in an unpatterned multilayer (only the Nb film was contacted), in which the critical

temperature is 0.2 K lower than that for the patterned devices ($T_C^{Nb(10)} = 3.0$ K), which could be due to a larger IEF from the unpatterned magnetic films. Figure 1(d) presents magnetic hysteresis data obtained by SQUID of the unpatterned structure at $T = 5$ K and $T = 12$ K. The coercive field value is the same for both GdN films and it increases as temperature is lowered. In other words, at temperatures above the Nb SC transition, the FI sandwich is always in the P state.

The patterned sample was then warmed up above $T_C^{Nb(10)}$ and cooled again while recording magnetoresistance (MR) curves with $I = 10$ μA and an in-plane magnetic field. A residual resistance in the AP state at the lowest temperature of $R_{res.1.3K}^{AP} = 0.05\,\Omega$ was observed and subtracted from all measurements shown in Figs. 2(a) and 2(b) for simplicity of analysis. As shown in Fig. 2(a), when the temperature reaches the superconducting transition of the Nb layer, the MR signal exhibits *sharp* switching between low and high resistance states. We attribute this change in resistance to result from the AP (low resistance) and P (high resistance) alignment of the GdN magnetizations, respectively, according to the spin switching effect.[14,15,20] No MR signal was observed for higher temperatures.

We note that the low resistance or R_{AP} state appears for small or no applied magnetic field. The MR loop is symmetric with respect to the field, and the low resistance region widens so the switching field value (H_{switch}) increases as the temperature decreases. Additionally, there is some hysteresis in H_{switch} as the values are 12.5 Oe higher on average for an increasing field sweep than for decreasing (see Fig. S.6 in the supplementary material).

Figure 2(b) plots resistance *vs* temperature at constant applied magnetic field, extracted from the MR data in Fig. 2(a). The curves exhibit a *sharp* jump from a high resistance state (R_P) to a low resistance state (R_P) at progressively lower temperatures as with increasing field.

We describe R_{AP} and R_P by the equation[22] $R(T) = \frac{R_N}{2}[1 + \tanh\frac{T - T_C}{\delta T}] + R_{offset}$, where R_N is the normal state resistance, T_C is the critical temperature, δT is the width of the transition, and R_{offset} is used to describe the R_P data at the lowest temperature. There is no offset resistance for R_{AP}, while $R_{offset}^P = 0.34\,\Omega$, which could be due to the stray-field (or dipolar coupling) between the two GdN layers suppressing superconductivity in the Nb layer.

We obtain $T_C^{AP} = 3.22$ K and $T_C^P = 2.5$ K, yielding a difference of $\Delta T_C \sim 0.7$ K, and a widening of the SC transition ($\delta T^{AP} = 0.24$ K and $\delta T^{AP} = 0.52$ K) due to the different IEFs induced by the GdN layers for both magnetic configurations.

The fact that the value of H_{switch} increases as temperature is lowered could be, at first glance, ascribable to the behavior for the upper critical field $H_{C2}(T)$. However, there are several features of our observations that do not support such assumptions: First, superconductors exhibit a smooth decrease in T_C and a broadening of the transition as field is increased, as opposed to sharp switching observed here. As shown in the supplementary material, we model the expected MR for our Nb layer by using the R(T) equation[22] and by linearly decreasing T_C from T_C^{AP} to T_C^P while increasing δT from δT^{AP} to δT^P. While the obtained curves are symmetric with H and the low resistance region widens with decreasing temperature, they do not account for the experimentally observed sharp, square-like switching. Second, we clearly observe a hysteresis in H_{switch}. Finally, assuming that H_{switch} is related to the upper critical field, such values are at least an order of magnitude too low for a 10 nm Nb film.[23]

Based on all these, we attribute the sharp switching in MR curves, the temperature dependence and hysteresis of H_{switch}, the reduced critical temperature of Nb, and the resistance of R_{AP} at low temperatures to the internal exchange field due to the proximity coupling with GdN layers in the sandwich[14,15,20] and an increasing antiferromagnetic (AF) coupling between FIs taking place through the SC Nb film as the temperature is lowered.[15,20]

The appearance of an AF coupling has been previously reported in GdN/Nb/GdN trilayers for temperatures below the SC transition of the Nb spacer.[15] As can be seen in our GdN/Nb/GdN trilayer control samples in the supplementary material, solely symmetric MR curves can be obtained for certain GdN and Nb thicknesses, as was seen for our JJ devices.

The SC transition temperature of the sandwiched Nb layer, the AF coupling strength, and its influence on the MR signal depend on the absolute and relative thicknesses of the GdN layers and the Nb spacer.[15] For different GdN and Nb thicknesses, the appearance of the AF coupling can be shifted further below the SC transition temperature so both remanent AP and P states can be obtained for some range of temperatures, which is desired for technological applications. However, in the case of our JJs, the thickness of the layers for which we achieve Josephson tunneling yields an AF coupling which prevents obtaining both remanent P and AP states.

We also determined the current-voltage (I-V) characteristics of our JJs by sweeping voltage and measuring the current through the device. Figure 3(a) plots I-V curves for the 10 μm junction at different temperatures and magnetic field values. As expected, for temperatures above $T_C^{Nb(10)}$, the junction presents no sign of Josephson current. However, at 1.3 K and zero-field, the junction presents a clear Josephson effect with a critical current of around 140 μA. Furthermore, if we use Fig. 2(a) as a guide, at 1.3 K, the zero-voltage state remains up to fields $\pm$250 Oe. In fact, the curve shown in Fig. 3(a) for 200 Oe differs very little from the I-V obtained with no applied field, whereas for 300 Oe, the critical current is strongly suppressed and the I-V
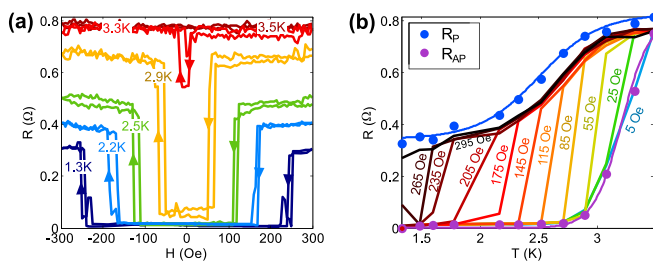

FIG. 2. (a) MR of a 10 μm device at different temperatures, exhibiting sharp switching between low and high resistance states. The curves are symmetric with field and are attributed to the SSE and an antiferromagnetic coupling between the GdN films through the superconducting Nb layer.[15,20] (b) Resistance *vs* temperature at different magnetic fields, constructed from the data in (a). The curves exhibit a sharp transition from a high (R_P) to a low resistance state (R_{AP}), which show a maximal difference in T_C of $\Delta T_C \sim 0.7$ K due to the SSE.

characteristics are closer to those of the normal state I-Vs (above 3.3 K). We ascertained that negative or positive fields as well as the magnetic history do not influence the I-Vs up to around 230 Oe at 1.3 K. For brevity, only positive field results are shown.

Figure 3(b) plots the dependence of the Josephson critical current I_C on the applied *in-plane* field (step size between 1 and 3 Oe) at $T = 1.3$ K. I_C is extracted at each field by fitting the I-V curve with $V = R_N \sqrt{I^2 - I_C^2}$ for $I \leq I_C$,[24] where R_N is the resistance of the junction in the normal state (see supplementary material). The inset of Fig. 3(b) shows the full range, where a sharp drop in critical current takes place at the switching field (around 250 Oe) between the AP and P states. As shown in Fig. 3(c), the I_C oscillations at low fields can be compared to the Airy pattern, theoretically expected for a circular junction.[3,25] I_C for fields below 60 Oe from Fig. 3(b) is normalized between 0 and 1 for simplicity and fit using the equation $|2\frac{J_1(x)}{x}|$, where J_1 is a Bessel function of first kind and $x = 2\pi(H - H_{off})/H_0$, where H_{off} is the shift in the field of the Fraunhofer pattern[17] and H_0 is the oscillation period. The results of the fitting are $H_0 = 14.9$ and $H_{off} = 3.8$ Oe. If we now take this value of H_0 and we consider that the flux through the junction obeys $\phi_0 = (2\lambda + t)d\mu_0 H_0$,[26] where ϕ_0 is the magnetic flux quantum, $t = 3$ nm the junction barrier thickness, and $d = 10\ \mu$m the junction diameter, we can estimate λ the average field penetration depth of the junction. We obtain $\lambda = 68$ nm, which is a reasonable result as it is an intermediate value of λ for the two different materials used as SC electrodes [$\lambda_{Nb} = 39$ nm[27] and $\lambda_{NbN} = 194$ nm (Ref. 28)]. Although the $I_C(H)$ dependence is far from a Fraunhofer pattern, some conclusions can be extracted if one zooms in the low-field region and I_C normalized [Fig. 3(c)]. First, one notes that the maximum is shifted

from zero field, which is a manifestation of the finite magnetization of the barrier GdN layer between the superconductors.[29] Second, although one distinguishes after normalization of the curve [see Fig. 3(c)] an oscillation of I_C that resembles the Airy pattern expected for circular Josephson junctions,[3] this pattern is distorted when the applied field gets larger. Moreover, the minima of I_C do not vanish at any field. These observations may be attributed to the highly asymmetric distribution of the current density through the junction. The asymmetry is field dependent: At very low fields, the junction is in a AF configuration, and one can assume that magnetic disorder is low. This may explain the "Fraunhofer-like" behavior of the $I_C(H)$ curve in Fig. 3(c) for $H < 40$ Oe. As the applied magnetic field becomes higher, it does not only affect the spatial behavior of the superconducting phase but also the magnetic configuration of the ferromagnetic layers. At higher field, the AF configuration becomes unstable and the GdN layers tend towards the P configuration and thus form a complex domain structure. Furthermore, in a multi-domain state, stray fields from the domain walls lead to a highly non-uniform superconducting order parameter, hence to a random interference pattern, and to the highly nonuniform current density.[29,30] This asymmetry could cause the non-vanishing minima of I_C.[3] The non-zero Josephson current in the AP state (fields above 250 Oe) is a result of the fitting, since it can be argued there is no Josephson current flowing from the curvature of the IV curve at $T = 1.3$ K and $H = 300$ Oe.

In conclusion, we have fabricated Josephson junction structures which incorporate an internal exchange-driven magnetic switch based on the superconducting spin switching effect. The use of ferromagnetic insulator layers to sandwich one of the superconducting electrodes of the junction, with one of the FI layers additionally acting as the JJ tunneling barrier, allows the control of the superconducting state of the sandwiched SC electrode through the interfacial exchange field. This control of the superconducting state results in a fully switchable Josephson junction, between superconductor-insulator-superconductor and superconductor-insulator-normal metal tunneling in the absence of an applied magnetic field. The vertical geometry of our device opens an opportunity to integrate such valves into superconducting circuits in analogy to magnetic tunnel junctions.[31] Moreover, by adding an additional FI layer in the same setup, one may be able to realize π– and φ_0–junctions predicted in recent works.[18,19] Different avenues will be explored to obtain non-volatile magnetic states to widen the potential applications of our device: further optimizing the GdN and Nb system, e.g., employing ultrathin FI layers to obtain out-of-plane anisotropies; varying the pillar geometry to introduce shape anisotropies and hard magnetic axes; and testing other superconducting materials with higher Tc as the core of the switch such as NbN and MgB$_2$.
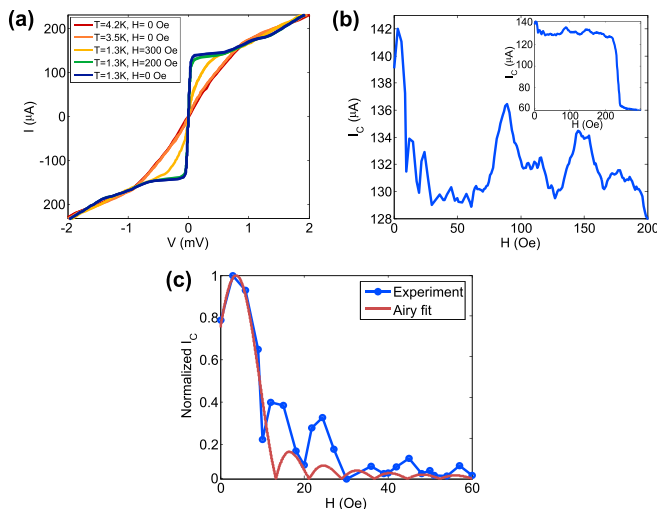

FIG. 3. (a) Current-voltage plots at different temperatures and applied magnetic fields for a 10 μm Josephson junction, with a maximum critical current $I_C = 142$ μA. (b) Field dependence of I_C at $T = 1.3$ K showing oscillations at fields below 200 Oe. The inset shows how I_C sharply drops at 250 Oe when the junction switches from the AP to the P state. (c) Fit of the Airy pattern expected for circular Josephson junctions to the normalized I_C at low fields, yielding a field period of $H_0 = 14.9$ Oe and an offset of $H_{off} = 3.8$ Oe.

See supplementary material for details about additional Josephson junction measurements, GdN/Nb/GdN control sample measurements, simulation of the effect of an external field on MR, and fitting equation to extract critical current from I-V plots.

REFERENCES

[1] B. Josephson, Phys. Lett. **1**, 251 (1962).

[2] B. D. Josephson, Rev. Mod. Phys. **46**, 251 (1974).

[3] A. Barone and G. Paterno, *Physics and Applications of the Josephson Effect* (Wiley Online Library, 1982), Vol. 1.

[4] A. I. Buzdin, Rev. Mod. Phys. **77**, 935 (2005).

[5] F. Bergeret, A. F. Volkov, and K. B. Efetov, Rev. Mod. Phys. **77**, 1321 (2005).

[6] A. Buzdin, Phys. Rev. Lett. **101**, 107005 (2008).

[7] M. Eschrig, Phys. Today **64**(1), 43 (2011); J. Linder and J. W. Robinson, Nat. Phys. **11**, 307 (2015).

[8] E. Gingrich, B. M. Niedzielski, J. A. Glick, Y. Wang, D. Miller, R. Loloee, W. Pratt, Jr., and N. O. Birge, Nat. Phys. **12**, 564 (2016).

[9] A. K. Feofanov, V. A. Oboznov, V. V. Bol'Ginov, J. Lisenfeld, S. Poletto, V. V. Ryazanov, A. N. Rossolenko, M. Khabipov, D. Balashov, A. B. Zorin *et al.*, Nature Phys. **6**, 593 (2010).

[10] X. Hao, J. S. Moodera, and R. Meservey, Phys. Rev. B **42**, 8235 (1990).

[11] B. Li, G.-X. Miao, and J. S. Moodera, Phys. Rev. B **88**, 161105 (2013).

[12] G.-X. Miao and J. S. Moodera, Phys. Chem. Chem. Phys. **17**, 751 (2015).

[13] E. Strambini, V. N. Golovach, G. De Simoni, J. S. Moodera, F. S. Bergeret, and F. Giazotto, Phys. Rev. Mater. **1**, 054402 (2017).

[14] B. Li, N. Roschewsky, B. A. Assaf, M. Eich, M. Epstein-Martin, D. Heiman, M. Münzenberg, and J. S. Moodera, Phys. Rev. Lett. **110**, 097001 (2013).

[15] Y. Zhu, A. Pal, M. G. Blamire, and Z. H. Barber, Nat. Mater. **16**, 195 (2017).

[16] M. Li, W. Cui, J. Yu, Z. Dai, Z. Wang, F. Katmis, W. Guo, and J. Moodera, Phys. Rev. B **91**, 014427 (2015).

[17] K. Senapati, M. G. Blamire, and Z. H. Barber, Nat. Mater. **10**, 849 (2011).

[18] F. S. Bergeret, A. Verso, and A. F. Volkov, Phys. Rev. B **86**, 060506 (2012); F. Bergeret, A. Verso, and A. F. Volkov, Phys. Rev. B **86**, 214516 (2012).

[19] M. A. Silaev, I. V. Tokatly, and F. S. Bergeret, Phys. Rev. B **95**, 184508 (2017).

[20] P. D. Gennes, Phys. Lett. **23**, 10 (1966).

[21] C. Delacour, L. Ortega, M. Faucher, T. Crozes, T. Fournier, B. Pannetier, and V. Bouchiat, Phys. Rev. B **83**, 144504 (2011).

[22] J. A. Burney, Ph.D. thesis, Stanford University, 2007.

[23] J. Quateman, Phys. Rev. B **34**, 1948 (1986).

[24] J. A. Glick, M. A. Khasawneh, B. M. Niedzielski, R. Loloee, W. P. Pratt, N. O. Birge, E. C. Gingrich, P. G. Kotula, and N. Missert, J. Appl. Phys. **122**, 133906 (2017).

[25] R. L. Peterson and J. W. Ekin, Phys. Rev. B **42**, 8014 (1990).

[26] M. Tinkham, *Introduction to Superconductivity* (Courier Corporation, 1996).

[27] B. W. Maxfield and W. L. McLean, Phys. Rev. **139**, A1515 (1965).

[28] B. Komiyama, Z. Wang, and M. Tonouchi, Appl. Phys. Lett. **68**, 562 (1996).

[29] T. S. Khaire, W. P. Pratt, and N. O. Birge, Phys. Rev. B **79**, 094523 (2009).

[30] M. A. Khasawneh, T. S. Khaire, C. Klose, W. P. Pratt, Jr., and N. O. Birge, Supercond. Sci. Technol. **24**, 024005 (2011).

[31] J. S. Moodera, L. R. Kinder, T. M. Wong, and R. Meservey, Phys. Rev. Lett. **74**, 3273 (1995).